


# Surface water productivity and sediment transport by Bering Strait throughflow in the Chukchi Shelf (the western Arctic Ocean) during the Holocene

The Holocene  
2018, Vol. 28(5) 814–826  
© The Author(s) 2017  
Reprints and permissions:  
sagepub.co.uk/journalsPermissions.nav  
DOI: 10.1177/0959683617744265  
journals.sagepub.com/home/hol  


Boo-Keun Khim,<sup>1</sup> Mi Jung Lee,<sup>2</sup> Hyen Goo Cho<sup>3</sup>  
and Kwangkyu Park<sup>1,4</sup>

## Abstract

Diverse paleoceanographic proxies from three sediment cores (GC12ex, JPC35, and JPC30) collected from the Chukchi Shelf north of the Bering Strait elucidate the Holocene paleoceanographic changes (surface water productivity and sediment transport) caused by the Bering Strait throughflow from the Bering Sea into the Chukchi Sea. Lithology of three sediment cores identified the same three units. Based on comparison and correlation to adjacent age-dated cores as well as AMS <sup>14</sup>C dates of core GC12ex, the boundary between Unit 1 and Unit 2a is dated about 8500 cal. yr BP, and the boundary between Unit 2a and Unit 2b is also dated about 4500 cal. yr BP. Consistent down-core profiles of the geochemical and isotopic properties among the three cores differentiate the paleoceanographic conditions corresponding to lithologic units. Based on the biogenic opal, total organic carbon, and  $\delta^{13}\text{C}$  values, Unit 1 is characterized by low surface water marine productivity under relatively shallow water with weak transport of Bering Strait throughflow. Unit 2a shows a mixture of terrestrial and marine contributions, indicating the onset of increased marine surface water productivity after the main flooding (~11,500 cal. yr BP) of the Bering Strait by the Holocene sea-level rise. Unit 2b exhibits stable and enhanced marine biogenic opal production similar to the present-day oceanographic conditions. Such paleoceanographic changes were confirmed by the clay minerals (smectite, illite, kaolinite, and chlorite) and detrital isotopes ( $\epsilon_{\text{Nd}}$  and  $^{87}\text{Sr}/^{86}\text{Sr}$ ). Thus, the Bering Strait throughflow played an important role on surface water productivity and sediment deposition in the Chukchi Shelf in response to Holocene sea-level rise after the opening of the Bering Strait.

## Keywords

Bering Strait, geochemistry, Holocene, isotope, paleoceanography, sea-level change, sediment source

Received 26 April 2017; revised manuscript accepted 12 October 2017

## Introduction

The Bering Strait is a shallow (about 50 m deep) and narrow (about 80 km wide) passage between Siberia and Alaska (Figure 1a). During the Quaternary, the Bering Strait played an important role in shaping the physiographic configuration of the shallow continental shelf areas occupying the Bering Sea and the Chukchi Sea (e.g. Hopkins, 1967, 1973). When the sea level was high, similar to the present-day conditions, during the interglacial periods, the shelf areas including the Bering Strait were submerged, linking the Bering Sea to the Chukchi Sea and forming a seawater gateway. In contrast, when the sea level was lower than the sill depth during the glacial periods, the Bering Sea was separated from the Chukchi Sea through the subaerial exposure of the shelf areas including the Bering Strait, resulting in the formation of the Bering Land Bridge (i.e. Beringia).

The sea-level change in the Bering Strait region is important for understanding the terrestrial and oceanographic conditions of Beringia (Hopkins, 1967, 1973). The continental shelf below the -120 m isobaths in the Bering Sea remained submerged throughout the last 25,000 years (Knebel, 1972). McManus and Creager (1984) reported that the Bering Strait was inundated by 14,400 <sup>14</sup>C yr BP since the Last Glacial Maximum. However, their sea-level chronology is problematic because the bulk sediments used

for radiocarbon age dating contained coal-like impurities. Based on AMS <sup>14</sup>C dates, Elias et al. (1996) suggested that a large portion of the Bering Strait region remained exposed above sea level until 11,000 <sup>14</sup>C yr BP, allowing human and animal migration between Asia and North America (e.g. Elias, 2001). Keigwin et al. (2006) argued that the Bering Strait may have been flooded between ca. 11,000 and 12,000 cal. yr BP, by providing the first marine evidence that Hope Valley (53 m deep) in the southern Chukchi Sea was invaded as early as 12,000 cal. yr BP based on

<sup>1</sup>Department of Oceanography, Pusan National University, Korea

<sup>2</sup>Division of Polar Earth-System Sciences, Korea Polar Research Institute, Korea

<sup>3</sup>Department of Earth and Environmental Sciences, Gyeongsang National University, Korea

<sup>4</sup>Division of Polar Paleoenvironment, Korea Polar Research Institute, Korea

## Corresponding author:

Boo-Keun Khim, Department of Oceanography, Pusan National University, Busan 46241, Korea.

Email: bkkhim@pusan.ac.kr

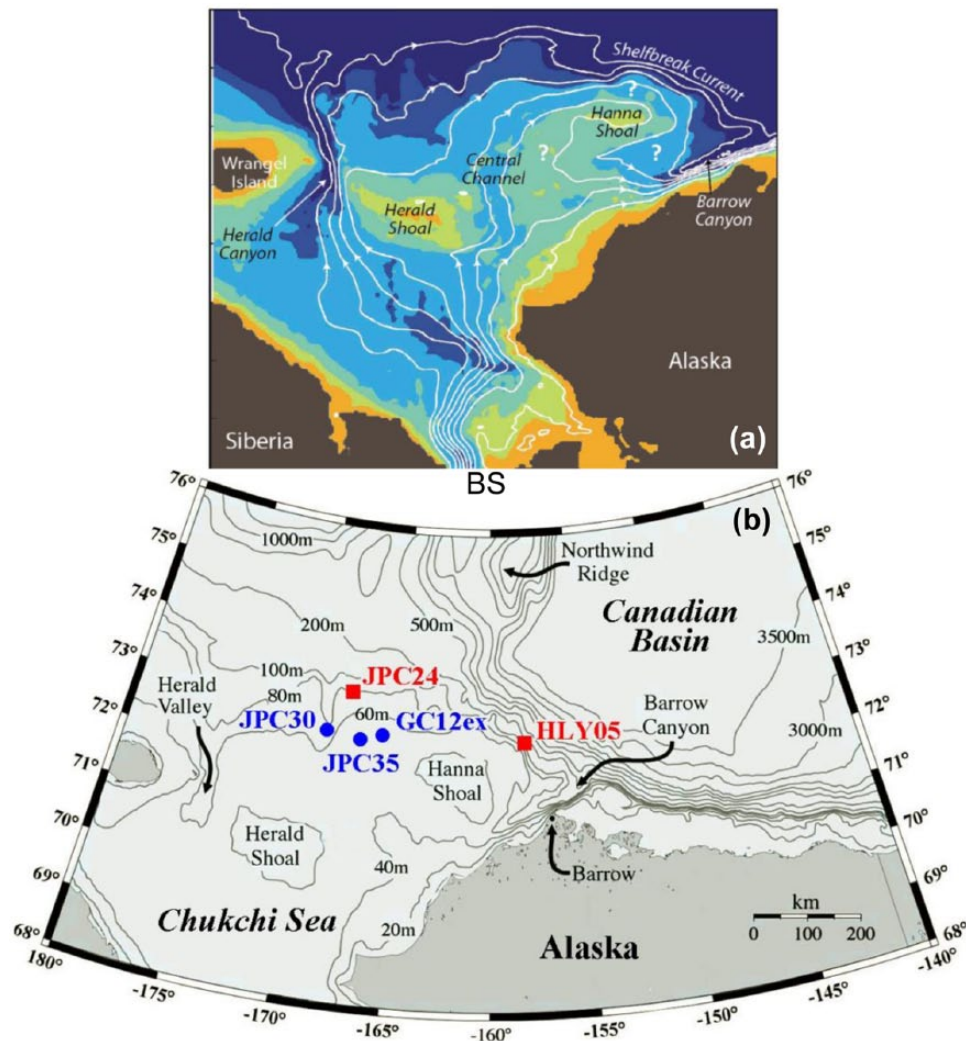


**Figure 1.** (a) Schematic pattern of the Bering Strait throughflow flowing out of the Bering Strait (BS) in the Chukchi Sea from the Bering Sea. (b) Collection sites of cores GC12ex, JPC35, JPC30, JPC24, and HLY05. Cores of blue dots are used in this study, and cores of red rectangles were adopted from Lundeen (2005) (for JPC24) and McKay et al. (2008) (for HLY05).

AMS  $^{14}\text{C}$  dates of foraminifera (*Elphidium excavatum*). Polyak et al. (2007) regarded Fe-oxide grains from cores sampled at the southern end of the Northwind Ridge in the western Arctic Ocean as a proxy for the Bering Strait source, suggesting that the most recent opening of the Bering Strait occurred during sea-level rise at around 12,000 cal. yr BP. Later, England and Furze (2008) confirmed that the Bering Strait was submerged by 11,500  $^{14}\text{C}$  yr BP by the presence of *Cyrtodaria kurriana* on northern Bank Island of the western Canadian Arctic Archipelago.

The North Pacific communicates with the Arctic Ocean through the Bering Strait which links the Bering Sea in the North Pacific to the Chukchi Sea in the Arctic Ocean. A steric height difference of about 0.5 m (equivalent to a sea-level slope of approximately  $10^{-6}$ ) between the Bering and Chukchi Seas was driven by a salinity difference between the fresher North Pacific Ocean and the saltier Arctic Ocean (Coachman et al., 1975; Stigebrandt, 1987), resulting in the northward mean flow. Thus, the Bering Strait throughflow is thought to transport a significant amount of fresh (i.e. less saline) North Pacific Water to the Arctic Ocean and then onto the North Atlantic (Woodgate and Aagaard, 2005). At present, the annual mean transport is estimated in the range of 0.6–0.9 Sv ( $10^6 \text{ m}^3$ ), with an average of  $0.8 \pm 0.1$  Sv (Aagaard et al., 1985; Roach et al., 1995; Woodgate and Aagaard, 2005). The transport variation is generally seasonal, smaller during winter because of more frequent storms, and larger during summer because of overall weaker winds (Aksenov et al., 2016;

Danielson et al., 2014). In addition, the reversed transport sometimes occurs during the particularly strong northerly winds for short days to week period (Woodgate et al., 2005).

The gateway position of the Bering Strait has played a significant role in controlling climate change by changing the volume of the Bering Strait throughflow. Several coupled global climate models have tested the importance of an open or closed Bering Strait to climatic variability in the North Atlantic (De Boer and Nof, 2004; Hu et al., 2010, 2012; Keigwin and Cook, 2007; Ortiz et al., 2012). For example, Keigwin and Cook (2007) suggested that when the Bering Strait is open, variability in the transport of relatively freshwater from the North Pacific to the North Atlantic through the Bering Strait may stabilize climatic variability in the North Atlantic. In contrast, when the Bering Strait was closed during the glacial periods, the absence of Bering Strait throughflow led to the occurrence of abrupt climate transition (e.g. Dansgaard-Oeschger and Heinrich events) (Hu et al., 2012). Recently, the model study by Ortiz et al. (2012) demonstrated a strong relationship between the Southern Ocean winds and the Bering Strait throughflow by showing that weak southern winds, followed by the cease of freshwater fluxes from the melting Laurentide Ice Sheet during the middle-Holocene, strengthened the Bering Strait throughflow.

Despite the potential significance of the Bering Strait, little is known about the paleoceanographic history in terms of surface water productivity and sediment transport before and after the

**Table 1.** Information of cores used in this study.

Core	Latitude (°N)	Longitude (°W)	Water depth (m)	Source
GC12ex	72°36.0'	166°00'	53	This study
JPC35	72°22.4'	168°04.2'	60	This study
JPC30	73°05.9'	168°25.3'	75	This study
JPC24	73°08.3'	167°31.7'	80	Lundeen (2005)
HLY05	72°41.4'	157°31.2'	415	McKay et al. (2008)

Holocene opening of the Bering Strait. Particularly, the Bering Strait throughflow has played an important role in delivering sea-water and sediments from the Bering Sea onto the Chukchi Shelf in response to the Holocene sea-level rise. The main objective of this study is to reveal the Holocene paleoceanographic changes in the Bering Strait area as indicated by geochemical/isotopic properties (surface water productivity) and clay minerals/detrital Nd/Sr isotopes (sediment transport) using three sediment cores recovered from the Chukchi Shelf (western Arctic Ocean).

## Materials and methods

Information on three sediment cores (MR06-04 GC12ex: GC12ex, HLY02-04 JPC30: JPC30, and HLY02-04 JPC35: JPC35) used in the present study and two published cores (HLY02-05 JPC24: hereafter JPC24; and HLY0501-05: hereafter HLY05) is summarized in Table 1. Two piston cores, JPC35 and JPC30, were obtained during cruise USCGC Healy 02-05 in 2002. A gravity core GC12ex was collected during cruise MR06-04 conducted by JAMSTEC in 2006. All cores were taken from the shallow Chukchi Shelf north of the Bering Strait (Figure 1b). Two cores, JPC24 (Lundeen, 2005) and HLY05 (McKay et al., 2008), taken in the study area were used to aid the age determination of our cores.

All cores were split onboard for lithologic description. In particular, preliminary sediment properties such as sediment color ( $b^*$ ) and magnetic susceptibility (MS;  $\kappa$ ) were measured onboard for core GC12ex. Sediment color was measured using a Minolta CM-2002 reflectance photospectrometer. MS was measured using a Bartington MS2C system with a loop sensor as part of the multi-sensor core logger. More information on core GC12ex can be found in the MR06-04 Leg. 2 Cruise Report ([http://www.godac.jamstec.go.jp/cruisedata/mirai/e/MR06-04\\_leg2.html](http://www.godac.jamstec.go.jp/cruisedata/mirai/e/MR06-04_leg2.html)). Sub-sampling for the laboratory experiments was carried out at JAMSTEC (for core GC12ex) and WHOI (for cores JPC35 and JPC30).

Geochemical properties of all three core sediments were measured at Pusan National University. Total carbon (TC) contents were measured using a Carlo Erba NA-1500 Elemental Analyzer. The analytical precision as a relative standard deviation ( $\pm 1\sigma$ ) is 1%. Total inorganic carbon (TIC) content was measured using an UIC CO<sub>2</sub> coulometer (Model CM5014). Assuming that all TIC is in the form of calcium carbonate, TIC content is converted to CaCO<sub>3</sub> content as a weight percentage using the multiplication factor 8.333 (a ratio of molecular weight between CaCO<sub>3</sub> and C). The analytical precision of TIC as a relative standard deviation ( $\pm 1\sigma$ ) is 2%. Total organic carbon (TOC) content was calculated by determining the difference between TC and TIC. Biogenic silica content was analyzed using a wet alkaline extraction method (DeMaster, 1981). The analytical precision as a relative standard deviation ( $\pm 1\sigma$ ) is 1%. Biogenic opal content was calculated by multiplying biogenic silica content by 2.4 (Mortlock and Froelich, 1989). Carbon isotopes ( $\delta^{13}\text{C}$ ) of sediment organic matter were measured using EA-IRMS (Europa Scientific 20–20 mass spectrometer) at Iso-Analytical Ltd., UK, after the acid-treatment of bulk sediments.  $\delta^{13}\text{C}$  values are expressed in conventional delta notation, which is the per mil deviation from the V-PDB. Precision for  $\delta^{13}\text{C}$  is about  $\pm 0.1\%$ .

The  $<2\ \mu\text{m}$  clay minerals in cores JPC35 and JPC30 were analyzed at Gyeongsang National University using a SIEMENS/BRUKER D5005 diffractometer with CuK $\alpha$  Ni-filtered radiations by X-ray diffraction on air-dried and ethylene-glycolated oriented mounts prepared by the 'smear-on-glass slide' method described by Stokke and Carson (1973). Clay minerals were identified following the classification of Brown and Brindley (1980) and Moore and Reynolds (1989). Semi-quantitative estimates (weighted peak area %) of major clay minerals (illite, smectite, kaolinite, and chlorite) were based on the method described by Biscaye (1965).

Nd and Sr isotope analyses of cores JPC35 and JPC30 were performed at Korea Polar Research Institute following standard techniques (Lee et al., 2011; Pin and Santos Zalduegui, 1997). Sequential extraction was performed to extract the detrital fraction from the sediment according to methods outlined by Bayon et al. (2002). Nd and Sr isotope measurements were conducted using a Thermo Finnigan TRITON thermal ionization mass spectrometer equipped with nine adjustable Faraday cups. Analytical precisions of the Sr and Nd isotope data are given as  $\pm 2\sigma$  standard errors ( $\pm 0.000004$ ). Mass fractionation correction was applied to the data by normalizing to  $^{86}\text{Sr}/^{88}\text{Sr} = 0.1194$  and  $^{146}\text{Nd}/^{144}\text{Nd} = 0.7219$  using an exponential law. Replicate analyses of standard NBS 987 and JNdi-1 Nd reference material gave  $^{87}\text{Sr}/^{86}\text{Sr} = 0.710260 \pm 4$  ( $n = 30$ ) and  $^{143}\text{Nd}/^{144}\text{Nd} = 0.510215 \pm 5$  ( $n = 30$ ). Procedural blanks were typically  $<70\ \text{pg}$  for Sr and  $30\ \text{pg}$  for Nd. The Nd isotopic composition was finally expressed as:

$$\epsilon_{\text{Nd}} = \left\{ \left( \frac{^{143}\text{Nd}}{^{144}\text{Nd}} \right)_{\text{Sample}} / \left( \frac{^{143}\text{Nd}}{^{144}\text{Nd}} \right)_{\text{CHUR}} - 1 \right\} \times 10^4$$

where CHUR stands for 'chondritic uniform reservoir'; that is,  $(^{143}\text{Nd}/^{144}\text{Nd})_{\text{CHUR}}$  is the value of the ratio in chondrites.

Because planktonic foraminiferal tests were rare and inadequate, AMS  $^{14}\text{C}$  ages of the acid-insoluble organic matter fraction of the five bulk sediments of core GC12ex were measured at the Rafter Radiocarbon Laboratory, Institute of Geological and Nuclear Sciences (New Zealand). A bivalve shell fragment at a depth of 300 cm was dated to provide additional dating information. We give AMS  $^{14}\text{C}$  ages as conventional (i.e. uncorrected)  $^{14}\text{C}$  yr BP (Table 2). These AMS  $^{14}\text{C}$  ages were calibrated to convert calendar year (cal. yr BP) with a reservoir effect of 400 years (e.g. McKay et al., 2008) using the CALIB Radiocarbon Calibration Program version 7.04 (Stuiver et al., 2017).

## Age estimate of core sediments

Based on onboard observation of sediment lithology and preliminary measurement of sediment properties (sediment color and MS), core GC12ex was divided into two major lithologic units at approximately 305 cm (an upper part as Unit 2 and a lower part as Unit 1) (Figure 2a and b). Unit 1 is characterized by low  $b^*$  and low MS values and is composed of slightly to moderately bioturbated dark lithic clayey silt with shell fragments. In contrast, Unit 2 is characterized by high  $b^*$  and high MS values and is composed of homogeneous to slightly bioturbated olive-gray diatom-bearing silty clay. Based on the variation in  $b^*$  and MS values, Unit 2

**Table 2.** Radiocarbon data for core GC12ex.

Depth (cm)	Sample type	Conventional $^{14}\text{C}$ age ( $^{14}\text{C}$ yr BP)	$\delta^{13}\text{C}$ (‰)	Calibrated $^{14}\text{C}$ age (cal. yr BP)	Calibrated $^{14}\text{C}$ age <sup>a</sup> (cal. yr BP)	Lab code
0	Bulk sediment	3336 ± 20	-22.2	3189 ± 20	689 ± 20	NZA35735
17	Bulk sediment	5054 ± 20	-22.1	5404 ± 20	3104 ± 20	NZA35736
87	bulk sediment	7089 ± 25	-22.7	7568 ± 25	4068 ± 25	NZA35737
202	Bulk sediment	10,539 ± 35	-23.6	11,785 ± 35	7285 ± 35	NZA35723
286	Bulk sediment	13,511 ± 45	-25.1	15,731 ± 45	8231 ± 45	NZA35724
300	Bivalve	8463 ± 25	0.2	9048 ± 25	9048 ± 25	NZA35703

<sup>a</sup>With local contamination offset (LCO) correction.

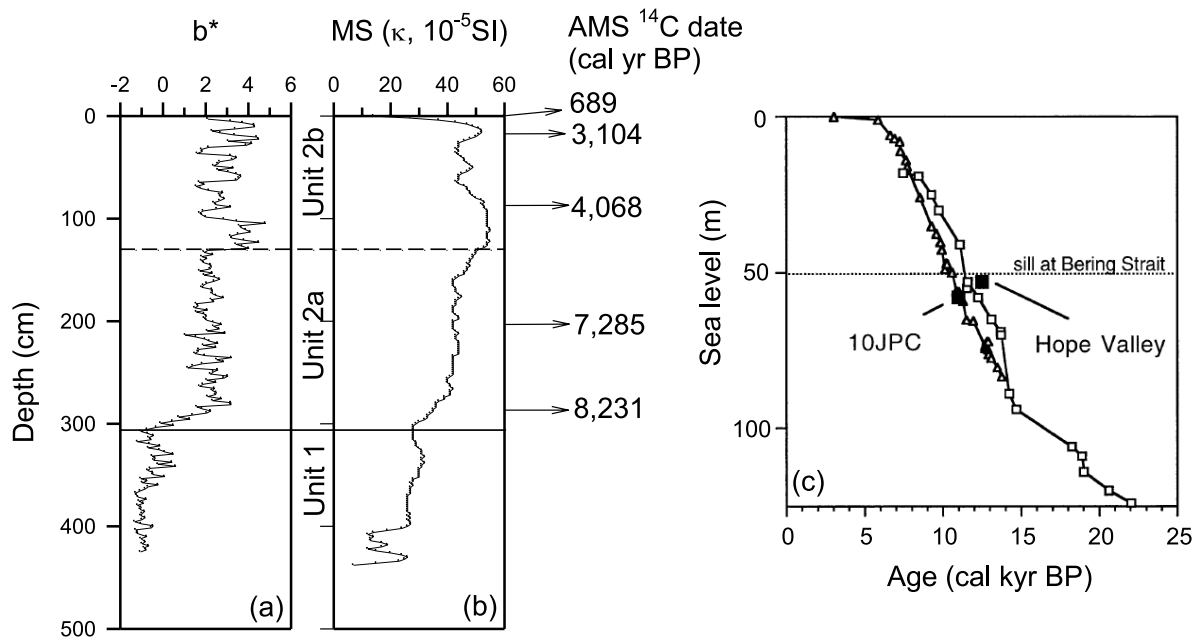


**Figure 2.** (a) Down-core profile of sediment color ( $b^*$ ) of core GC12ex. (b) Down-core profile of magnetic susceptibility (MS) of core GC12ex. Lithologic units (Unit 1, Unit 2a, and Unit 2b) are defined by these sediment properties. AMS  $^{14}\text{C}$  dates (calibrated calendar year with LCO correction) are also denoted. (c) New sea-level curve in the Chukchi Sea (Keigwin et al., 2006).

can be further subdivided at about 130 cm into the upper Unit 2b and the lower Unit 2a (Figure 2a and b). Unit 2b shows higher  $b^*$  and MS values with more variation than Unit 2a.

A prerequisite for paleoceanographic reconstruction based on core sediments is the establishment of a reliable age model. For example, multiple down-core AMS  $^{14}\text{C}$  measurements have commonly constrained the age of late Pleistocene sediment cores in the western Arctic Ocean (e.g. Darby et al., 1997). Five AMS  $^{14}\text{C}$  ages of the bulk sediments in core GC12ex are listed in Table 2. No age reversal was observed, resulting in a reasonable stratigraphic order corresponding to the lithologic units. The AMS  $^{14}\text{C}$  measurements were performed on acid-insoluble organic matter of the bulk sediments. Because fresh (autochthonous) organic matter is likely to dissolve in HCl and  $\text{HNO}_3$ , the acid-insoluble organic matter seems to contain old allochthonous (continental) organic matter. Thus, radiocarbon dating of this organic matter is likely to reflect a maximum (i.e. oldest) age for the bulk sediments.

It is not surprising, then, that the age of the core top is 3336  $^{14}\text{C}$  yr BP by AMS  $^{14}\text{C}$  dating of bulk sediments. Local contamination by fossil organic matter from sediments containing older carbon is a commonly observable problem in radiocarbon age dating (e.g. Nelson et al., 1988). We refer to this age difference as 'local contamination offset' (LCO), as treated similarly in the Antarctic Ocean (e.g. Hillenbrand et al., 2009). After calibration of AMS  $^{14}\text{C}$  ages, we corrected LCO under assumption that  $\delta^{13}\text{C}$  values may indicate the degree of LCO. Compared with the core top

( $\delta^{13}\text{C} = -22.2\%$  and  $\text{LCO} = 2500$ ), LCO of each dating horizon was calculated by  $\Delta\delta^{13}\text{C}$  relative to the core-top value which may be proportional to the degree of LCO. These LCO-corrected AMS  $^{14}\text{C}$  ages were shown in Figure 2a. This correction seems manipulated and unacceptable to decide the precise and real age. At this situation, thus, the sediment age estimated straightforward by direct AMS  $^{14}\text{C}$  dating is difficult or almost impossible in constraining the precise age of the sediment core. Nonetheless, an orderly succession of five AMS  $^{14}\text{C}$  ages guarantees the context of age range to determine the probable age of the lithologic units. Another assumption is that a part of the core top may be lost during the retrieval of gravity core, which is usually observed during the execution. In general, the core-top sediments were missing when the piston or gravity corer was retrieved. In this study, because we did not take multiple cores, we cannot judge whether our gravity core preserves the complete core top. Thus, core-top missing may be another reason for the old age at the core top.

For the purpose of validating the reasonably probable age estimates of the lithologic boundaries, we adopted the indirect approach. The  $\delta^{13}\text{C}$  profiles of the sediment organic matter from our studied cores were compared precisely with those of well-dated sediment cores (JPC24 and HLY05) from the study area (Figure 3).  $\delta^{13}\text{C}$  values of all cores range between  $-25.3\%$  and  $-22.0\%$ . The  $\delta^{13}\text{C}$  profiles show similar upward increasing patterns toward the core top. Unit 1 shows consistently low  $\delta^{13}\text{C}$  values ( $-25.3\%$  to  $-24.6\%$ ) in all cores (Figure 3). Unit 2a is characterized by a rapid increase (from  $-24.6\%$  to  $-22.9\%$ ) in



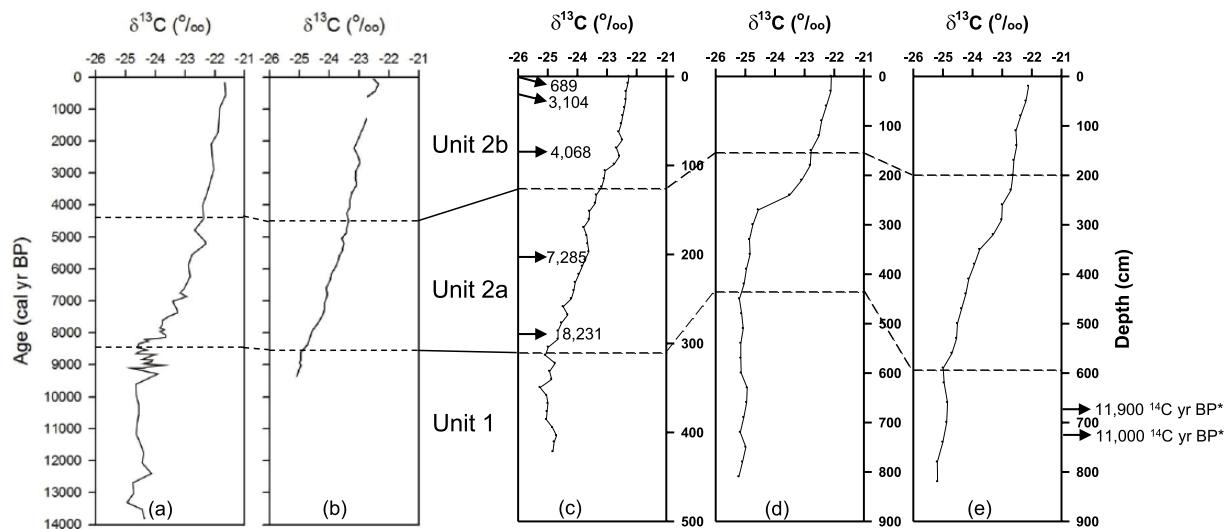


**Figure 3.** Age estimates of lithologic boundaries for the studied cores (GC12ex, JPC35, and JPC30) based on the correlation of the  $\delta^{13}\text{C}$  values of the sediment organic matter with those of the well-dated core (JPC24 and HLY05) chronology. The  $\delta^{13}\text{C}$  chronology was adopted from Lundeen (2005) for core JPC24 and McKay et al. (2008) for core HLY05, respectively. Five AMS  $^{14}\text{C}$  dates (calibrated calendar year with LCO correction) of core GC12ex and two AMS  $^{14}\text{C}$  dates (measured  $^{14}\text{C}$  yr\*) at the bottom of core JPC30 (Hill and Driscoll, 2010) are shown: (a) JPC24, (b) HLY05, (c) GC12ex, (d) JPC35 and (e) JPC30.

$\delta^{13}\text{C}$  values, whereas Unit 2b is characterized by stable and high  $\delta^{13}\text{C}$  values with a little gradual increase between  $-22.9\%$  and  $-22.0\%$  (Figure 3). Based on the correlation of  $\delta^{13}\text{C}$  values among these cores, the lithologic boundary between Unit 1 and Unit 2a is judged at approximately 8500 cal. yr BP from cores JPC24 and HLY05 (Lundeen, 2005; McKay et al., 2008). This age seems to correspond to the LCO-corrected AMS  $^{14}\text{C}$  age ( $>8241$  cal. yr BP) (Figure 2b). The age difference may be attributed to slight error of LCO correction. An age of bivalve shell fragment measured at 300 cm just above the lithologic boundary (305 cm) of core GC12ex is 9048 cal. yr BP (Table 2). A little older age is a result that this shell fragment is reworked. In addition, Kim et al. (2017) divided three palynological zones from a core (ARA02B-01A) collected in the northern margin of Chukchi Shelf and, conclusively, their lower lithologic boundary ( $\sim 8400$  cal. yr BP) is matched thoroughly with the age estimate between Unit 1 and Unit 2a.

Hill and Driscoll (2010) reported two AMS  $^{14}\text{C}$  dates (11,900  $^{14}\text{C}$  yr BP for 680 cm and 11,000  $^{14}\text{C}$  yr BP for 720 cm) for the bottom part of core JPC30, which is the same core in this study (Figure 4c). Although these ages are reversed because of the vital effect difference in radiocarbon fractionation between foraminifera and mollusks (Hill and Driscoll, 2010), these AMS  $^{14}\text{C}$  dates were older than the estimated age of unit boundary (approximately 8500 cal. yr BP), which confirms that the age of Unit 1 in our cores is appropriate. Gusev et al. (2009) investigated new boreholes and seismic reflection data from the upper Holocene sediments clearly related to the postglacial transgression in the southwestern Chukchi Sea between the mainland and Wrangel Island, and reported a decrease (from  $\sim\text{m/kyr}$  to  $\sim\text{cm/kyr}$ ) in the sedimentation rate during the early stages of flooding (ca. 9000  $^{14}\text{C}$  yr BP). Additionally, Bauch et al. (2001) observed fluvial-type deposition prior to 8900 cal. yr BP on the Siberian margin (about 31 m deep) of the Laptev Sea, which is a little shallower than the water depth of cores in the Chukchi Shelf. This transition is coincident with the increase in the  $\delta^{13}\text{C}$  values of organic matter by the sudden decrease in the input of terrestrial organic matter from rivers and coastal erosion (Bauch et al., 2001). These previous results (Bauch et al., 2001; Gusev et al., 2009; Hill and Driscoll, 2010; Keigwin et al., 2006) in the western Arctic Ocean corroborate the age boundary between Unit 1 and Unit 2a of our cores (Figure 3).

Using the same approach with  $\delta^{13}\text{C}$  data from cores JPC24 and HLY05 (Lundeen, 2005; McKay et al., 2008), the lithologic boundary between Unit 2a and Unit 2b was correlated at about 4500 cal. yr BP (Figure 3), which coincides with the LCO-corrected AMS  $^{14}\text{C}$  age ( $<4068$  cal. yr BP) (Figure 2). The upper palynological zone of a core (ARA02B-01A) in the northern margin of Chukchi Shelf was dated at about 4000 cal. yr BP (Kim et al., 2017). Lisé-Pronovost et al. (2009) reported a major decrease (from  $\sim 3.5$  m/kyr to  $\sim 1.2$  m/kyr) in the sedimentation rate on the Arctic Alaskan margin at approximately 5000 cal. yr BP. The average sedimentation rate of shelf sediments on the Laptev Sea margin also began to decrease at about 5000 cal. yr BP when the modern sea level was established in Arctic Siberia (Bauch et al., 2001). This timing is also consistent with sea-level records from Beringia (Elias et al., 1996; Mason and Jordan, 2002). The coincidence between our age expectation and the well-dated cores by previous studies (Bauch et al., 2001; Kim et al., 2017; Lisé-Pronovost et al., 2009) guarantees a plausible and acceptable age estimate for the lithologic boundary between Unit 2a and Unit 2b, which is indicative of depositional environment changes, although this age postdates a little the timing when the sea level reached the present condition (Figure 2c).

## Results

Biogenic opal and TOC contents of the three sediment cores (GC12ex, JPC35, and JPC30) from the Chukchi Shelf, as shown in Figure 4, represent the level of primary productivity in the surface water. Biogenic opal content of all cores varies from 1% to 18%, and TOC content ranges from 0.2% to 1.8% (Figure 4). It is particularly noteworthy that all down-core profiles of biogenic opal and TOC contents are remarkably consistent (i.e. an upward increasing trend). Unit 1 ( $>\text{ca. } 8500$  cal. yr BP) is characterized by consistently low biogenic opal (1–7%) and TOC (0.2–1.2%) contents along with low  $\delta^{13}\text{C}$  values (Figure 3). Biogenic opal and TOC contents show the upward gradual increase in Unit 2a (from ca. 8500 to ca. 4500 cal. yr BP), ranging from 5% to 12% and from 1.0% to 1.6%, respectively, in all cores, a trend also observable clearly in the  $\delta^{13}\text{C}$  profiles (Figure 3). Unit 2b (from ca. 4500 cal. yr BP to the present) is characterized by high biogenic opal (10–18%) and TOC (1.1–1.8%) contents along with high  $\delta^{13}\text{C}$  values ( $-22.9\%$ – $-22.0\%$ ; Figure 3). The down-core variation in

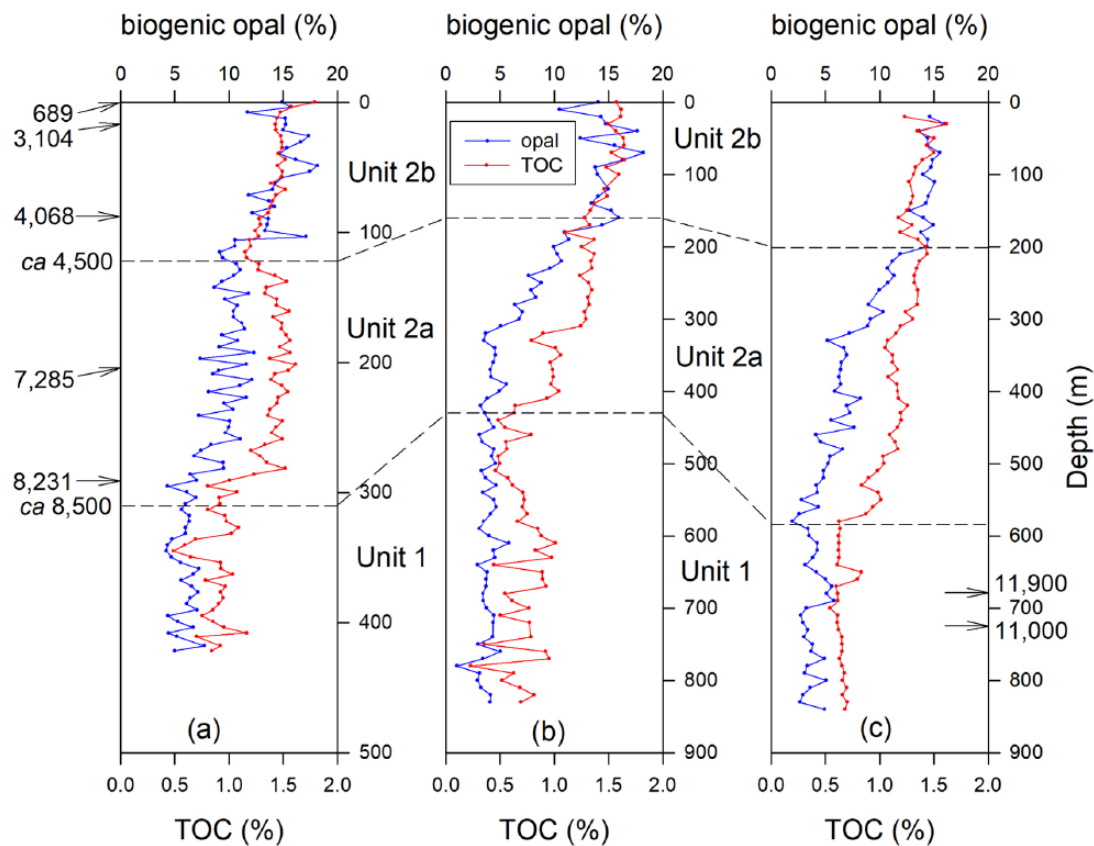


**Figure 4.** Down-core profiles of biogenic opal and TOC (total organic carbon) contents in (a) core GCI2ex, (b) core JPC35, and (c) core JPC30. Unit boundaries (dash lines) and their age estimates are indicated based on Figures 2 and 3. Five AMS  $^{14}\text{C}$  dates (calibrated calendar year with LCO correction) of core GCI2ex and two AMS  $^{14}\text{C}$  dates (measured  $^{14}\text{C}$  yr) at the bottom of core JPC30 (Hill and Driscoll, 2010) are shown.

biogenic opal and TOC contents is highlighted in Figure 7, which exhibits that the clusters of biogenic opal and TOC contents are separated distinctly in terms of individual lithologic unit.

As shown in Figure 5, the fine-grained fraction of core sediments consists of four major clay minerals (smectite, illite, kaolinite, and chlorite). Two cores (JPC35 and JPC30) show similar proportion of clay minerals (illite: 60% vs 58%, chlorite: 20% vs 23%, kaolinite: 11% vs 11%, and smectite: 9% vs 9%) and that their variation is not clear throughout the depth. The order of dominant clay minerals in both cores is same as reported by the previous studies (Naidu and Mowatt, 1983; Naidu et al., 1982). In contrast to the down-core variation of each clay mineral amount, smectite/illite (S/I) ratio and chlorite/kaolinite (C/K) ratio reflect that down-core variation is different with lithologic unit. Similar to the division by the geochemical properties (biogenic opal and TOC), S/I and C/K ratios of core JPC35 and S/I ratio of core JPC30 are low for Unit 1, increasing for Unit 2a, and high for Unit 2b, although C/K ratio of core JPC30 is likely dissimilar (Figure 5b and d).

$\epsilon_{\text{Nd}}$  values and Sr isotopic compositions of detrital fraction in cores JPC35 and JPC30 show a similar pattern to those of the S/I and C/K ratios, although some discrepancy was observed (Figure 6a and b).  $\epsilon_{\text{Nd}}$  values for cores JPC35 and JPC30 vary between  $-10.6$  and  $-8.8$  and between  $-9.9$  and  $-9.1$ , respectively, and  $^{87}\text{Sr}/^{86}\text{Sr}$  ratios for both cores are in the ranges between 0.7118 and 0.7161 and between 0.7115 and 0.7149, respectively.  $\epsilon_{\text{Nd}}$  values for core JPC35 are overall low ( $\sim -10.0$ ) in Unit 1 and Unit 2a, with minimum record around 200 cm, and higher ( $\sim -9.0$ ) in Unit 2b.  $\epsilon_{\text{Nd}}$  values for core JPC30 show an increasing trend throughout the core and no distinct variation pattern different from those observed in core JPC35.  $^{87}\text{Sr}/^{86}\text{Sr}$  ratios for core JPC35 show an opposite trend to the  $\epsilon_{\text{Nd}}$  values, with high values (0.713–0.716)

for Unit 1, low values ( $\sim -0.712$ ) for Unit 2b, and a gradual decrease (from 0.716 to 0.712) for Unit 2a. Although general trend of  $^{87}\text{Sr}/^{86}\text{Sr}$  ratios for core JPC30 follows core JPC35, showing the upward decreasing trend (from 0.714 to 0.711),  $^{87}\text{Sr}/^{86}\text{Sr}$  ratios of Unit 1 are a little higher than those of core JPC35.

## Discussion

### Holocene paleoceanographic changes in the Chukchi Shelf

Keigwin et al. (2006) revealed that the flooding of the Chukchi Shelf (approximately 50 m) and the Bering Strait by glacio-eustatic sea-level rise may have occurred between ca. 11,000 and 12,000 cal. yr BP. The marine geophysical CHIRP sub-bottom data by Hill and Driscoll (2008) suggested that regional transgression across the interflues on the middle Chukchi Shelf probably postdated approximately 11,500  $^{14}\text{C}$  yr BP, which corresponds to Meltwater Pulse 1B. It also coincides with a second smaller negative  $\delta^{18}\text{O}$  excursion (about 12,000–13,000 cal. yr BP) of planktonic foraminifera observed in cores from the Chukchi Borderland (Polyak et al., 2007). After the main flooding of the Bering Strait at approximately 11,500  $^{14}\text{C}$  yr BP, the onset of seawater and sediment transport from the Bering Sea onto the Chukchi Shelf may have occurred by the Bering Strait throughflow. Such an influx of relatively fresh North Pacific water through the Bering Strait by the Bering Strait throughflow may also have played an important role in affecting the strength of the halocline in the western Arctic Ocean, as it does today (Danielson et al., 2014).

Although the age estimates in the present study are relatively circumstantial, the lithology of the three sediment cores can be divided into three units (Units 1, 2a, and 2b; Figure 2). Unit 1

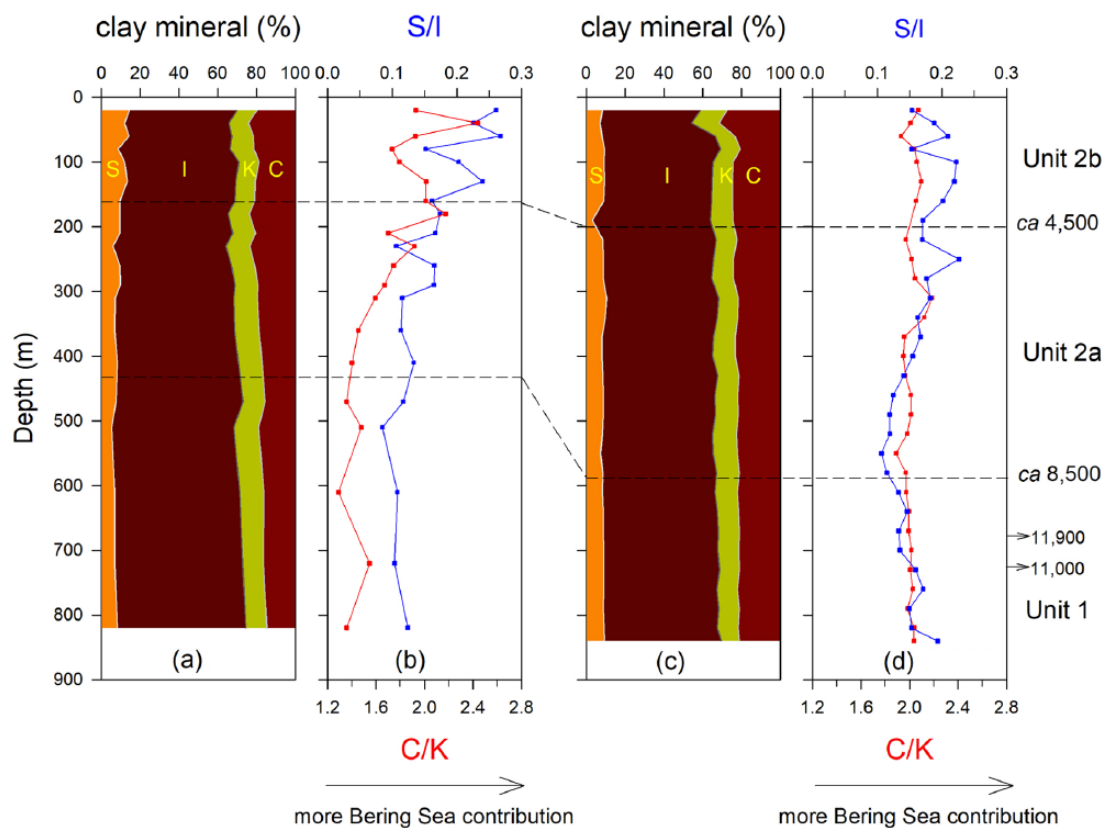


**Figure 5.** Down-core profiles of (a) proportion of each clay mineral (S: smectite, I: illite, K: kaolinite, C: chlorite) and (b) S/I and C/K ratios of core JPC35; and (c) proportion of each clay mineral and (d) S/I and C/K ratios of core JPC30. Unit boundaries (dash lines) and their age estimates refer to Figures 2 and 3. Two AMS <sup>14</sup>C dates (measured <sup>14</sup>C yr) at the bottom of core JPC30 (Hill and Driscoll, 2010) are shown.

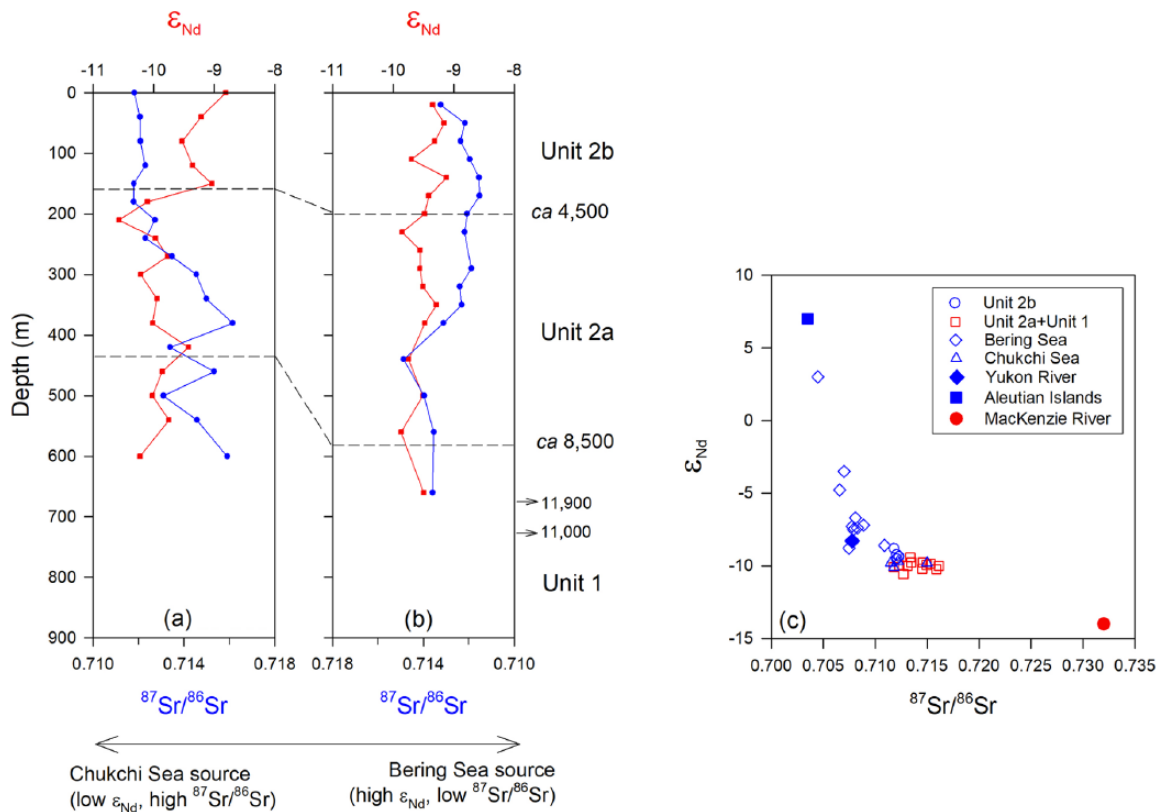


**Figure 6.** Down-core profiles of (a) ε<sub>Nd</sub> values and <sup>87</sup>Sr/<sup>86</sup>Sr ratios of core JPC35 and (b) ε<sub>Nd</sub> values and <sup>87</sup>Sr/<sup>86</sup>Sr ratios of core JPC30. High ε<sub>Nd</sub> values and low <sup>87</sup>Sr/<sup>86</sup>Sr ratios are originated from the Bering Sea source, whereas low ε<sub>Nd</sub> values and high <sup>87</sup>Sr/<sup>86</sup>Sr ratios are derived from the Chukchi Sea source (Asahara et al., 2012). Unit boundaries (dash lines) and their age estimates are indicated based on Figures 2 and 3. Two AMS <sup>14</sup>C dates (measured <sup>14</sup>C yr) at the bottom of core JPC30 (Hill and Driscoll, 2010) are shown. (c) The relationship between ε<sub>Nd</sub> values and <sup>87</sup>Sr/<sup>86</sup>Sr ratios of cores JPC35 and JPC30. All other isotope data of the Bering Sea and the Chukchi Sea with the end-members (Yukon River, Aleutian Islands, MacKenzie River) are adopted from Asahara et al. (2012).

(before approximately 8500 cal. yr BP) shows low  $\delta^{13}\text{C}$  values (Figure 3) as well as low biogenic opal and TOC contents (Figure 4), suggesting that the terrestrial contribution of organic matter overwhelmed marine production, even though sea level had increased to flood the Bering Strait (Keigwin et al., 2006). The major sediment sources for the Arctic Alaskan margin including the Chukchi Shelf have been diverse since the marine transgression of the Chukchi Shelf associated with the last deglaciation. In addition to sediment transport from the Bering Sea, these include river discharge, coastal erosion, and the redistribution of sediment by ice drift. In particular, Hill and Driscoll (2008) emphasized that smaller rivers in northwest Alaska served as a network of submarine paleochannels, playing an important role in delivering sediments to the northeast Chukchi Sea during the last deglaciation.

A flooding surface of post-transgressive marine sediment identified from the CHIRP sub-bottom profiles (Hill and Driscoll, 2008, 2010) lies in the lower part of Unit 2a and above Unit 1 in cores JPC35 and JPC30. The flooding surface was formed during a rapid sea-level rise, recording the transition to more open marine conditions. Hill and Driscoll (2010) also found abundant *Elphidium excavatum* below the flooding surface, which are indicative of brackish/estuarine environments, coincident with the preservation of blueschist metamorphic minerals (e.g. glaucophane, epidote). This unit includes a large amount of terrigenous components likely transported from the nearby Brooks Range of northern Alaska, which is characterized by widespread blueschist bedrocks (Dusel-Bacon et al., 1989). According to borehole and seismic reflection study in the southwestern Chukchi Sea (Gusev et al., 2009), the early Holocene sediments reveal fairly high sedimentation rates (~m/kyr) because of the early stage of Arctic shelf flooding (e.g. Stein et al., 2004) that resulted in the rapid sediment filling of local seafloor depressions by the reworking of deposits. This indicates that Unit 1 was formed under relatively very shallow water conditions characterized by greater terrestrial input from the nearby Alaskan continent.

Unit 2 is subdivided into the upper Unit 2b and the lower Unit 2a on the basis of the variation pattern of  $b^*$  and MS values (Figure 2). Unit 2a (from ca. 8500 to ca. 4500 cal. yr BP) is characterized by the noticeable increase of biogenic opal, TOC, and  $\delta^{13}\text{C}$  values (Figures 3 and 4). The increasing trend of all these geochemical and isotope values indicates the shift of organic matter flux from decreasing terrestrial supply to increasing marine surface water production in association with the rising sea level during the Holocene. McKay et al. (2008) reported an increase in the  $\delta^{13}\text{C}$  values of core HLY05 (Figure 1b) on the Alaskan margin in the eastern Chukchi Sea from the early to late-Holocene at about 8500 cal. yr BP (Figure 3b), which is consistent with the decrease in C/N ratios and pollen concentrations. The mean  $\delta^{13}\text{C}$  values for organic matters of marine origin are  $-20\%$ , while those of terrestrial origin are  $-27\%$  (Hedges and Parker, 1976). Bauch et al. (2001) also found the similar increase in  $\delta^{13}\text{C}$  values toward more marine conditions on the Siberian margin of the Laptev Sea at around 7200 cal. yr BP, which is coincident with the main shift from a freshwater-dominated diatom assemblage to a marine-dominated diatom imprint at a break in average sedimentation rate. The delayed timing (7200 cal. yr BP) on the Siberian margin may be because of the shallow depth (about 31 m deep) of the studied cores, which are therefore likely influenced by greater terrestrial sediment contribution (Bauch et al., 2001). The increasing pattern of TOC content in Unit 2a is likely different from that of the biogenic opal content (Figure 4), which may be attributed to the additional increased contribution of terrestrial organic carbon reworked from the coastal areas of Alaska. The clusters of the biogenic opal and TOC contents are distinctly separated, representing each unit (Figure 7). Unit 2a, which is clearly transitional between Unit 1 (low biogenic opal and TOC) and Unit 2b (high biogenic opal and TOC), supports mixing between terrestrial input and the marine contribution to biogenic

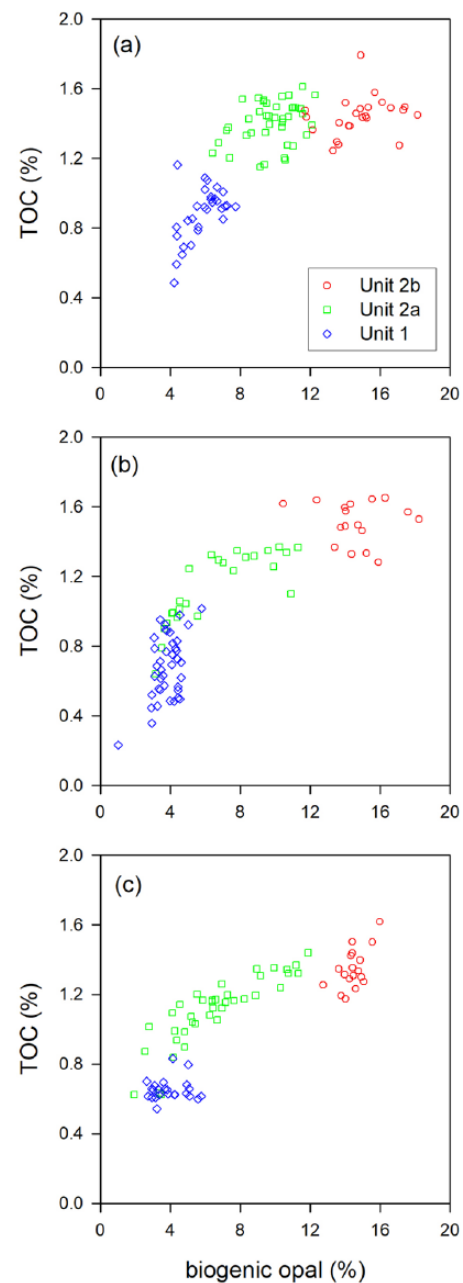


**Figure 7.** Relationship between biogenic opal content and total organic carbon (TOC) in the lithologic units (Unit 2b: red circle; Unit 2a: green rectangle; Unit 1: blue diamond) of (a) core GC12ex, (b) core JPC35, and (c) core JPC30. Note that each unit is distinguished clearly by the relationship of these geochemical properties.

production during the middle-Holocene when sea level is still rising (Figure 7).

In the Chukchi Sea, Keigwin et al. (2006) showed that brownish to olive-gray, strongly bioturbated mud (i.e. postglacial sediments corresponding to Unit 1) overlies stiffer grayish, sometimes laminated mud containing ice rafted debris (i.e. glacial/deglacial sediments corresponding to Unit 2). The lithologic change associated with the transition from deglacial to marine Holocene environments has been related to Holocene paleoceanographic changes on the Arctic continental margins (e.g. Darby et al., 1997; Lisé-Pronovost et al., 2009; Polyak et al., 2007). Bauch et al. (2001) reported a major change in hydrology and depositional environment at around 9000 cal. yr BP for the modern 30-m isobath in the Siberian margin of the Laptev Sea. It highlights the strong decline in sediment transfer to the outermost shelf and slope because of a further decrease of the shelf gradient and the



long distance from the coast. The Holocene sediments of core HLY05 from the Arctic Alaskan margin also recorded a drop in the amount of terrestrial organic material reworked from the peatlands of the Bering Land Bridge, including the Chukchi Shelf and the Alaska coastline that were inundated during the postglacial period (McKay et al., 2008).

During the early to middle-Holocene, several pieces of evidence for the oceanographic and environmental change were reported in the Chukchi Sea. The maximum reversed gradient between  $\delta^{18}\text{O}$  values and planktonic foraminifera size observed in the Chukchi Sea occurred between ca. 9000 and 7000 cal. yr BP (Hillaire-Marcel et al., 2004). They interpreted that this indicates significantly enhanced inflow of the warm Atlantic Water to the Arctic Ocean, resulting in a strong stratification of the surface water layer. de Vernal et al. (2005) revealed the Holocene variability of sea ice cover in the Chukchi Sea (western Arctic Ocean), showing that a slight warming of surface waters was indicated by the maximum dinoflagellate cyst concentrations and the change in the coarse silt–sand fraction. This coincides with the maximum inflow of the Atlantic Water at around 8000 cal. yr BP, prior to the stabilization of sea level close to its present limit on the Chukchi Shelf (Hillaire-Marcel et al., 2004). This is also closely related to relatively less saline seawater into the Chukchi Sea of the western Arctic Ocean delivered by Bering Strait throughflow (Keigwin et al., 2006). Thus, Unit 2a seems to correspond to the interval of rapid sea-level rise during the early to middle-Holocene (Bard et al., 1998; Mason and Jordan, 2002; Mueller-Lupp et al., 2000).

The sediments of Unit 2b (from ca. 4500 cal. yr BP to the present day) contain higher biogenic opal and TOC contents (Figure 4) and higher  $\delta^{13}\text{C}$  values than do those of Units 2a and 1 (Figure 3). This indicates a high level of marine production, similar to present-day conditions. Thus, the geochemical properties of Unit 2b signify that the Bering Strait throughflow under warm climatic conditions sustained high marine production in surface water of the Chukchi Sea (Codispoti et al., 2005; Grebmeier et al., 2006). Hill and Driscoll (2008) found that the late-Holocene deposits were acoustically laminated, with low reflectivity because the sediments are composed of silty clay. During the late-Holocene, sea level likely reached the present-day level before 5000 cal. yr BP to complete the modern physiographic configuration in the Bering Sea and Chukchi Sea (Keigwin et al., 2006). A decrease in the average sedimentation rate occurred, and the late-Holocene constant sedimentation rate was stabilized on the Siberian margin of the Laptev Sea at about 5100–5300 cal. yr BP, close to the Holocene sea-level highstand (Bauch et al., 2001). Lisé-Pronovost et al. (2009) also reported that a major decrease in the sediment supply on the continental shelf near Barrow Canyon began at around 5000 cal. yr BP. Age estimate of about 5000 cal. yr BP is consistent with sea-level records from farther east in Beringia (Elias et al., 1996; Mason and Jordan, 2002). Net flow through the Bering Strait has transported water and sediment continuously to the Chukchi Sea. Nelson and Creager (1977) reported that an increased amount of sediment from the Yukon River was deposited in the Bering Sea after approximately 5000 cal. yr BP, but argued that about a third of the sediment load from the Yukon River may have been transported into the Chukchi Sea. Therefore, the sediments from the Bering Sea were deposited continuously onto the Chukchi Shelf during the last 4500 years after the Holocene sea-level highstand was nearly established, as evidenced by the geochemical properties of Unit 2b (Figures 4 and 7).

#### *Sediment transport by the Bering Strait throughflow from the Bering Sea onto the Chukchi Shelf*

In the Bering and Chukchi Seas, clay mineral distribution of the surface sediments has been well studied (e.g. Naidu and Mowatt, 1983; Naidu et al., 1982). Clay mineral compositions of surface

sediments in the Bering Sea are governed by their sources and surface current patterns. The major provenances of smectite in the Bering Sea are the volcanic mafics of the Aleutian Island Arc, the Kamchatka Peninsula, and the Alaska Peninsula, along with a relatively minor source represented by the Yukon River drainage basin (Naidu et al., 1982). The known major provenances of illite are the Koryak Mountains, east Siberia (Chukotsk), and western Alaska (Hathon and Underwood, 1991). In the Bering Sea, chlorite-bearing sediments were supplied by the physical weathering of metasedimentary and plutonic rocks in Alaska, and kaolinite rich sediments were supplied from the kaolinite-bearing paleosols and shales of northern Alaska (Naidu et al., 1982). Given the potential sources and prevailing current systems, smectite-rich clays are transported northward to the Bering Strait from the Aleutian Island Arc (Naidu et al., 1982). Although most smectite from the Yukon River is deposited near the river mouth, the remainder is also dispersed northward along the coast by the Alaskan Coastal Current, and eventually conveyed through the Bering Strait to the Chukchi Sea (McManus et al., 1974).

The clay mineral smectite serves as an indicator for sediment source areas on the circum-Arctic continental shelves, including the Chukchi Sea (Dethleff et al., 2000; Kalinenko, 2001; Khim, 2003; Nurnberg et al., 1995; Nwaodua et al., 2014; Viscosi-Shirley et al., 2003; Wahsner et al., 1999). For example, the eastern Kara Sea and the western Laptev Sea are dominated by high amounts of smectite, whereas the continental shelves from the eastern Laptev Sea over the Siberian and Chukchi Seas to the Canadian Beaufort Sea in the western Arctic Ocean are characterized by relatively low smectite concentrations (Darby, 1975; Darby et al., 2011; Wahsner et al., 1999). Khim (2003) reported that smectite content increases significantly toward the western Chukchi Sea far from the Long Strait in the East Siberian Sea, and suggested that this peculiar pattern can only be explained by an input of smectite from the Bering Strait. Based on diffuse spectral reflectance of Quaternary sediments from the Northwind Ridge (western Arctic Ocean), Yurco et al. (2010) proposed that the smectite and chlorite in the Chukchi Sea were derived from the Bering Sea. Nwaodua et al. (2014) also reported that the high amount of smectite and chlorite were distributed north of the Bering Strait. The central Chukchi Sea is apparently a major depositional repository of smectite derived from the Bering Sea, compared with other sources in the western Arctic Ocean. This implies that the closing of the Bering Strait during periods of low sea level restricted the deposition of smectite and chlorite, compared with other clay minerals, from the Bering Sea in the Chukchi Sea.

Smectite/illite (S/I) and chlorite/kaolinite (C/K) ratios for cores JPC35 and JPC30 show the depositional history in accordance with the opening of the Bering Sea in response to Holocene sea-level rise (Figure 5). Low S/I and C/K ratios for Unit 1 before approximately 8500 cal. yr BP can be explained by a lower supply of sediments including smectite and chlorite from the Bering Sea because of the shallow water depth of Bering Strait, although the Bering Strait was open to flood. The steady deposition of smectite and chlorite, resulting in the gradual increase of S/I and C/K ratios, began after the main flooding of the Bering Strait which predated the lithologic boundary between Unit 1 and Unit 2 by 3 kyr. Geochemical properties of these cores also confirm the increased influx from the Bering Sea, which causes enhanced marine production in the surface waters (Figure 4). High S/I and C/K ratios for Unit 2b indicate more delivery of smectite-rich and chlorite-rich clays since ~4500 cal. yr BP, which may be attributed to more influx of Bering Strait throughflow. This coincides with the high biogenic opal and TOC contents, which reflect greater marine production similar to present-day conditions. The reason for the different pattern of S/I and C/K ratios between cores JPC35 and JPC30 is not clear (Figure 5), but it may be attributed partly to the different water depth between two cores sites, which results in the

local effect of different depositional process. Otherwise, the hydrographic flow patterns to transport the sediment particles may not be identical between two core sites.

Ortiz et al. (2009) reported high amounts of chlorite and muscovite on the Chukchi–Alaskan margin near Barrow Canyon during the middle-Holocene (approximately 6000–3600 cal. yr BP). Ortiz et al. (2009) followed the geographic distribution of clay minerals reported by Kalinenko (2001), suggesting that chlorite and muscovite are effective tracers of North Pacific water from the Bering Sea. Ortiz et al. (2009) measured the diffuse spectral reflectance of sediments and quantified the clay minerals from raw XRD data using the RockJock computer program (Eberl, 2003). Their XRD analysis was actually conducted for the size fraction <4 mm, including silt-sized particles. In addition, according to this XRD analytical method, abundance of smectite is underestimated. This is the primary reason that smectite was not discussed in Ortiz et al. (2009). Large amounts of chlorite and muscovite were observed between approximately 6000 and 3600 cal. yr BP (Ortiz et al., 2009). This corresponds to Unit 2a of the studied cores, which, based on geochemical properties, is characterized by increased marine influence (Figure 4). However, chlorite content of our cores is not as high as Ortiz et al. (2009), despite the gradual increase (Figure 5). Considering the location (72°30.7'N, 157°2.1'W) and water depth (673 m) of core HLY0501-JPC6 analyzed by Ortiz et al. (2009), an increase in chlorite and muscovite during the middle-Holocene may be an increased supply from northwest Alaska (Naidu and Mowatt, 1983; Naidu et al., 1982) in addition to an increase in the inflow of North Pacific water through the Bering Strait. Otherwise, the different analytical method of clay mineral quantification is an alternative reason. Ortiz et al. (2009) measured the diffuse spectral reflectance of sediments and quantified the clay minerals from raw XRD data using the RockJock computer program (Eberl, 2003). Their XRD analysis was actually conducted for the size fraction <4 mm, including silt-sized particles. However, small abundance (less than 1–2%) of smectite can be identified using this XRD analytical method. This is the primary reason that smectite was not explained in Ortiz et al. (2009). More research is required to clarify the differences of the observations and conclusions between Ortiz et al. (2009) and the present study.

Like clay minerals, Sr and Nd isotopes of the detrital fractions have been used as tracers to identify the provenance of marine sediments (e.g. Asahara et al., 1999; Fagel et al., 2014; Nakai et al., 1993; Winter et al., 1997). Asahara et al. (2012) reported that Sr isotope ( $^{87}\text{Sr}/^{86}\text{Sr}$ ) ratios of the surface sediments in the Chukchi Sea (0.711–0.715) are higher than those in the Bering Sea (0.705–0.711), whereas  $\epsilon_{\text{Nd}}$  values in the Chukchi Sea (–10.1 to –8.3) are lower than those in the Bering Sea (–8.6 to 3.0). This may indicate either that the sediments in the Bering Sea and Chukchi Sea were transported from distinctly different sources or that the source signatures have altered through a change in weathering.

The detrital particles in the Chukchi Sea are potentially transported from the North American continent through the Mackenzie River, from eastern Siberia by the Siberian Coastal Current, and from the Bering Sea by the Bering Strait inflow (Darby, 1975; Darby et al., 2009; Hill and Driscoll, 2010; Khim, 2003; McManus et al., 1974; Naidu et al., 1982; Nelson and Creager, 1977; Polyak et al., 2007; Viscosi-Shirley et al., 2003; Wahsner et al., 1999; Yurco et al., 2010). The Mackenzie River basin in North America preserves the Proterozoic and Archean crusts of the Canadian Shield, and thus,  $^{87}\text{Sr}/^{86}\text{Sr}$  ratios of these old continental crusts are relatively high (0.732–0.734) and  $\epsilon_{\text{Nd}}$  values are relatively low (–14.7 to –13.7) (Millot et al., 2003). Bedrock  $^{87}\text{Sr}/^{86}\text{Sr}$  ratios (0.711) are lower and  $\epsilon_{\text{Nd}}$  values (–9.0) are higher in northeastern Siberia off the western Chukchi Sea than those of the Canadian Shield because the Cretaceous igneous and metamorphic rocks in

northeastern Siberia are younger than the Canadian Shield (e.g. Amato et al., 2003). Because the Transport Drift in the Arctic Ocean delivers most sediments from the Siberia to the central Arctic region and ultimately North Atlantic, Beaufort Gyre is the dominant agent transporting the sediment from the Canadian areas including Alaska to the Chukchi Sea. Therefore, the detrital particles from the circum-Arctic Ocean to the Chukchi Sea are characterized by high  $^{87}\text{Sr}/^{86}\text{Sr}$  ratios and low  $\epsilon_{\text{Nd}}$  values.

Figure 6c shows that the detrital particles delivered by the Bering Strait throughflow from the Bering Sea are differentiated into two different components: the continental component from the Yukon River and the Aleutian Arc volcanic component (Asahara et al., 2012; Hathon and Underwood, 1991; Naidu and Mowatt, 1983; Naidu et al., 1982; Sancetta et al., 1985). The Yukon River basin in Alaska consists mainly of Mesozoic and Paleozoic sedimentary rocks, characterized by fairly low  $^{87}\text{Sr}/^{86}\text{Sr}$  ratios (0.708–0.709) and high  $\epsilon_{\text{Nd}}$  values (–7.5 to –6.7) (GEOROC, 2003). The isotopic compositions of the Aleutian volcanic arc are distinct, showing very low  $^{87}\text{Sr}/^{86}\text{Sr}$  ratios (0.703–0.704) and very high  $\epsilon_{\text{Nd}}$  values (–8 to –6) (GEOROC, 2003). Therefore, the detrital sediments transported by the Bering Strait inflow from the Bering Sea to the Chukchi Sea are characterized by low  $^{87}\text{Sr}/^{86}\text{Sr}$  ratios and high  $\epsilon_{\text{Nd}}$  values.

The  $\epsilon_{\text{Nd}}$  values and  $^{87}\text{Sr}/^{86}\text{Sr}$  ratios of cores JPC35 and JPC30 show that a depositional history is consistent with the clay minerals (Figure 6), although the  $\epsilon_{\text{Nd}}$  values of core JPC30 show the dissimilar pattern. Same as C/K ratio of core JPC30, such difference may be because of the local different depositional conditions between two core sites. Higher  $^{87}\text{Sr}/^{86}\text{Sr}$  ratios and lower  $\epsilon_{\text{Nd}}$  values within Unit 1 are primarily attributed to the greater contribution of sediments from the Chukchi–Alaskan margin just after the opening of the Bering Strait. The decrease in the  $^{87}\text{Sr}/^{86}\text{Sr}$  ratios and the increase in the  $\epsilon_{\text{Nd}}$  values within Unit 2a can be explained by the gradual increase in sediments delivered from the Bering Sea by the Bering Strait throughflow after the main flooding of the Bering Strait. The consistently low  $^{87}\text{Sr}/^{86}\text{Sr}$  ratios and high  $\epsilon_{\text{Nd}}$  values within Unit 2b indicate an equilibrium of sediment contributions from the Bering Sea during the last 4500 years, since the Holocene sea level reached present-day conditions (Keigwin et al., 2006). This isotopic signature of the depositional history coincides with the Holocene paleoceanographic changes in surface water conditions evidenced by the geochemical properties.

## Conclusion

Three sediment cores (GC12ex, JPC35, and JPC30) collected from the Chukchi Shelf north of the Bering Strait record the Holocene paleoceanographic changes caused by the transport of seawater and sediments from the Bering Sea into the Chukchi Sea by the Bering Strait throughflow in response to the opening of the Bering Strait. The lithologic boundary was estimated by the correlation of the  $\delta^{13}\text{C}$  profiles of the sedimentary organic matter with those of adjacent age-dated cores as well as AMS  $^{14}\text{C}$  dates: approximately 8500 cal. yr BP between Unit 1 and Unit 2a and about 4500 cal. yr BP between Unit 2a and Unit 2b. Based on biogenic opal and TOC contents and  $\delta^{13}\text{C}$  values of sediment organic matter of the three cores, Unit 1 (until approximately 8500 cal. yr BP) is characterized by a greater terrestrial contribution with weaker marine production, indicating low sea-level conditions. Unit 2a (approximately 8500–4500 cal. yr BP) is characterized by a mixture of terrestrial and marine contributions, with increased marine productivity, reflecting rising sea-level conditions. In contrast, Unit 2b (approximately 4500 cal. yr BP to the present) indicates stable marine conditions with high biogenic opal production and TOC preservation, similar to present-day high sea-level conditions. Smectite/illite (S/I) and chlorite/kaolinite (C/K) ratios,  $\epsilon_{\text{Nd}}$  values, and  $^{87}\text{Sr}/^{86}\text{Sr}$

ratios of detrital particles from cores JPC35 and JPC30 also confirm the paleoceanographic changes, showing the sediment deposition from more Chukchi Sea-derived particles through the mixture of particles from the Chukchi Sea and Bering Sea toward more Bering Sea-derived particles onto the Chukchi Shelf before and after the Holocene opening of the Bering Strait. Finally, the Bering Strait throughflow has played an important role in delivering the seawater and sediment particles from the Bering Sea to the Chukchi Shelf to control the depositional history and paleoceanographic changes in response to Holocene sea-level rise.

### Acknowledgements

Professor L. Keigwin (WHOI), the captain, crew, and all on-board researchers of the USCGC Healy 02-05 cruise as well as Dr N. Harada (JAMSTEC), the captain, crew, and all on-board researchers of the MR04-06 cruise are thanked for core sampling. We appreciate the sampling of sediments from cores JPC35 and JPC30 by Ms Ellen Roosen (WHOI). Two anonymous reviewers and Dr Fabienne Marret (associate editor) are greatly appreciated for their constructive comments to improve the data interpretation.

### Funding

This research was supported by the Polar Academic Program (PAP to BKK) and partly by the National Research Foundation of Korea grant (2016R1A2B4008256 to BKK).

### References

- Aagaard K, Roach AT and Schumacher JD (1985) On the wind-driven variability of the flow through Bering Strait. *Journal of Geophysical Research* 90: 7213–7221.
- Aksenov Y, Karcher M, Proshutinsky A et al. (2016) Arctic pathways of Pacific Water: Arctic Ocean model intercomparison experiments. *Journal of Geophysical Research* 121: 27–59.
- Amato JM, Miller EL, Wright JE et al. (2003) Dike swarms on Seward Peninsula, Alaska, and their implications for the kinematics of Cretaceous extension in the Bering Strait region. *Canadian Journal of Earth Sciences* 40: 865–886.
- Asahara Y, Takeuchi F, Nagashima K et al. (2012) Provenance of terrigenous detritus of the surface sediments in the Bering and Chukchi Seas as derived from Sr and Nd isotopes: Implications for recent climate change in the Arctic regions. *Deep Sea Research Part II* 61–64: 155–171.
- Asahara Y, Tanaka T, Kamioka H et al. (1999) Provenance of the north Pacific sediments and process of source material transport as derived from Rb–Sr isotope systematics. *Chemical Geology* 158: 271–291.
- Bard E, Arnold M, Hamelin B et al. (1998) Radiocarbon calibration by means of mass spectrometric  $^{230}\text{Th}/^{234}\text{U}$  and  $^{14}\text{C}$  ages of corals: An updated database including samples from Barbados, Mururoa and Tahiti. *Radiocarbon* 40: 1085–1092.
- Bauch HA, Mueller-Lupp T, Taldenkova E et al. (2001) Chronology of the Holocene transgression at the North Slope margin. *Global and Planetary Change* 31: 125–139.
- Bayon G, German CR, Boella RM et al. (2002) An improved method for extracting marine sediment fractions and its application to Sr and Nd isotopic analysis. *Chemical Geology* 187: 179–199.
- Biscaye PE (1965) Mineralogy and sedimentation of recent deep sea clay in the Atlantic Ocean and adjacent seas and oceans. *Geological Society of America Bulletin* 76: 803–832.
- Brown G and Brindley GW (1980) X-ray diffraction procedures for clay mineral identification. In: Brindley GW and Brown G (eds) *Crystal Structures of Clay Minerals and Their X-ray Identification*. London: Mineralogical Society of London, pp. 305–359.
- Coachman LK, Aagaard K and Tripp RB (1975) *Bering Strait: The Regional Oceanography*. Seattle, WA: University of Washington Press, 172 pp.
- Codispoti LA, Flagg C, Kelly V et al. (2005) Hydrographic conditions during the 2002 SBI process cruises. *Deep Sea Research Part II* 52: 3199–3226.
- Danielson SI, Weingartner TJ, Hedstrom KS et al. (2014) Coupled wind-forced controls of the Bering–Chukchi shelf circulation and the Bering Strait throughflow: Ekman transport, continental shelf waves, and variations of the Pacific–Arctic sea surface height gradient. *Progress in Oceanography* 125: 40–61.
- Darby DA (1975) Kaolinite and other clay minerals in Arctic Ocean sediments. *Journal of Sedimentary Petrology* 45: 272–279.
- Darby DA, Bischof JF and Jones GA (1997) Radiocarbon chronology of depositional regimes in the western Arctic Ocean. *Deep Sea Research Part I* 44: 1745–1757.
- Darby DA, Myers WB, Jakobsson M et al. (2011) Modern dirty sea ice characteristics and sources: The role of anchor ice. *Journal of Geophysical Research* 116: C09008.
- Darby DA, Ortiz J, Polyak L et al. (2009) The role of currents and sea ice in both slowly deposited central Arctic and rapidly deposited Chukchi–Alaskan margin sediments. *Global and Planetary Change* 68: 58–72.
- De Boer AM and Nof D (2004) The Bering Strait’s grip on the northern hemisphere climate. *Deep Sea Research Part I* 51: 1347–1366.
- de Vernal A, Hillaire-Marcel C and Darby DA (2005) Variability of sea ice cover in the Chukchi Sea (western Arctic Ocean) during the Holocene. *Paleoceanography* 20: PA4018.
- DeMaster DJ (1981) The supply and accumulation of silica in the marine environment. *Geochimica et Cosmochimica Acta* 5: 1715–1732.
- Dethleff D, Rachold V, Tintelnot M et al. (2000) Sea-ice transport of riverine particles from the Laptev Sea to Fram Strait based on clay mineral studies. *Canadian Journal of Earth Sciences* 89: 496–502.
- Dusel-Bacon C, Brosgé WP, Till AB et al. (1989) Distribution, facies, ages, and proposed tectonic associations of regionally metamorphosed rocks in northern Alaska. *US Geological Survey Professional Paper 1497-A*, 73pp.
- Eberl DD (2003) *User guide to RockJock – A program for determining quantitative mineralogy from X-ray diffraction data*. Open File Report 03-78, 40pp.
- Elias SA (2001) Beringian paleoecology: Results from the 1997 workshop. *Quaternary Science Reviews* 20: 7–13.
- Elias SA, Short SK, Nelson CH et al. (1996) Life and times of the Bering land bridge. *Nature* 382: 60–63.
- England JH and Furze MFA (2008) New evidence from the western Canadian Arctic Archipelago for the resubmergence of Bering Strait. *Quaternary Research* 70: 60–67.
- Fagel N, Not C, Gueibe J et al. (2014) Late Quaternary evolution of sediment provenances in the Central Arctic Ocean: Mineral assemblage, trace element composition and Nd and Pb isotope fingerprints of detrital fraction from the Northern Mendeleev Ridge. *Quaternary Science Reviews* 92: 140–154.
- GEOROC (2003) Geochemistry of rocks of the oceans and continents. Mainz, Germany, Max-Planck Institute für Chemie. Available at: <http://georoc.mpch-mainz.gwdg.de/>.
- Grebmeier JM, Cooper LW, Feder HM et al. (2006) Ecosystem dynamics of the Pacific influenced Northern Bering and Chukchi Seas. *Progress in Oceanography* 71: 331–361.
- Gusev EA, Andreeva IA, Anikina NY et al. (2009) Stratigraphy of Late Cenozoic sediments of the western Chukchi Sea: New results from shallow drilling and seismic-reflection profiling. *Global and Planetary Change* 68: 115–131.

- Hathon EG and Underwood MB (1991) Clay mineralogy and chemistry as indicators of hemipelagic sediment dispersal south of the Aleutian arc. *Marine Geology* 97: 145–166.
- Hedges JI and Parker PL (1976) Land-derived organic matter in surface sediments from the Gulf of Mexico. *Geochimica et Cosmochimica Acta* 40: 1019–1029.
- Hill JC and Driscoll NW (2008) Paleodrainage on the Chukchi shelf reveals sea level history and meltwater discharge. *Marine Geology* 254: 129–151.
- Hill JC and Driscoll NW (2010) Iceberg discharge to the Chukchi shelf during the Younger Dryas. *Quaternary Research* 74: 57–62.
- Hillaire-Marcel C, de Vernal A, Polyak L et al. (2004) Size-dependent isotopic composition of planktic foraminifers from Chukchi Sea vs. NW Atlantic sediments – Implications for the Holocene paleoceanography of the western Arctic. *Quaternary Science Reviews* 23: 245–260.
- Hillenbrand CD, Smith JA, Kuhn G et al. (2009) Age assignment of a diatomaceous ooze deposited in the western Amundsen Sea embayment after the last glacial maximum. *Journal of Quaternary Science* 25: 280–295.
- Hopkins DM (1967) Quaternary marine transgressions in Alaska. In: Hopkins DM (ed.) *The Bering Land Bridge*. Stanford, CA: Stanford University Press, pp. 47–90.
- Hopkins DM (1973) Sea level history in Beringia during the past 250,000 years. *Quaternary Research* 3: 520–540.
- Hu A, Meehl GA, Han W et al. (2012) Role of the Bering Strait on the hysteresis of the ocean conveyor belt circulation and glacial climate stability. *Proceedings of National Academy of Sciences of the United States of America* 109: 6417–6422.
- Hu A, Meehl GA, Otto-Bliensner BL et al. (2010) Influence of Bering Strait flow and North Atlantic circulation on glacial sea-level changes. *Nature Geoscience* 3: 118–121.
- Kalinenko VV (2001) Clay minerals in sediments of the Arctic Seas. *Lithology and Mineral Resources* 36: 362–372.
- Keigwin LD and Cook MS (2007) A role for North Pacific salinity in stabilizing North Atlantic climate. *Paleoceanography* 22: PA3102.
- Keigwin LD, Donnelly JP, Cook MS et al. (2006) Rapid sea-level rise and Holocene climate in the Chukchi Sea. *Geology* 34: 861–864.
- Khim BK (2003) Two modes of clay-mineral dispersal pathways on the continental shelves of the East Siberian Sea and western Chukchi Sea. *Geosciences Journal* 7: 253–262.
- Kim SY, Polyak L and Delusina I (2017) Terrestrial and aquatic palynomorphs in Holocene sediments from the Chukchi-Alaskan margin, western Arctic Ocean: Implications for the history of marine circulation and climatic environments. *The Holocene* 27: 976–986.
- Knebel HJ (1972) *Holocene sedimentary framework of the East-Central Bering Sea continental shelf*. PhD Thesis, University of Washington, 86 pp.
- Lee MJ, Lee JI, Kwon S-T et al. (2011) Sr-Nd-Pb isotopic compositions of submarine alkali basalts recovered from the South Korea Plateau, East Sea. *Geosciences Journal* 15: 149–160.
- Lisé-Pronovost A, St-Onge G, Brachfeld S et al. (2009) Paleomagnetic constraints on the Holocene stratigraphy of the Arctic Alaskan margin. *Global and Planetary Change* 68: 85–99.
- Lundeen Z (2005) *Elemental and isotopic constraints on the Late Glacial–Holocene transgression and paleoceanography of the Chukchi Sea*. MS Thesis, University of Massachusetts Amherst, 91 pp.
- McKay JL, de Vernal A, Hillaire-Marcel C et al. (2008) Holocene fluctuations in Arctic sea-ice cover: Dinocyst-based reconstructions for the eastern Chukchi Sea. *Canadian Journal of Earth Sciences* 45: 1377–1397.
- McManus DA and Creager JS (1984) Sea-level data for parts of the Bering–Chukchi shelves of Beringia from 19,000 to 10,000 14C yr. B.P. *Quaternary Research* 21: 317–325.
- McManus DA, Venkataratnam K, Hopkins DM et al. (1974) Yukon River sediment of the northern most Bering Sea shelf. *Journal of Sedimentary Petrology* 44: 1052–1060.
- Mason OK and Jordan JW (2002) Minimal late-Holocene sea level rise in the Chukchi Sea: Arctic insensitive to global change. *Global and Planetary Change* 32: 13–23.
- Millot R, Gaillardet J, Dupré B et al. (2003) Northern latitude chemical weathering rates: Clues from the Mackenzie River Basin, Canada. *Geochimica et Cosmochimica Acta* 67: 1305–1329.
- Moore DM and Reynolds RC (1989) *X-ray Diffraction and the Identification and Analysis of Clay Minerals*. Oxford: Oxford University Press, 332 pp.
- Mortlock RA and Froelich PN (1989) A simple method for the rapid determination of biogenic opal in pelagic marine sediments. *Deep Sea Research Part A* 36: 1415–1426.
- Mueller-Lupp T, Bauch HA, Erlenkeuser H et al. (2000) Changes in the deposition of terrestrial organic matter on the Laptev Sea shelf during the Holocene: Evidence from stable carbon isotopes. *International Journal of Earth Sciences* 89: 563–568.
- Naidu AS and Mowatt TC (1983) Sources and dispersal patterns of clay minerals in surface sediments from the continental-shelf areas off Alaska. *Geological Society of America Bulletin* 94: 841–854.
- Naidu AS, Creager JS and Mowatt TC (1982) Clay mineral dispersal patterns in the north Bering and Chukchi Seas. *Marine Geology* 47: 1–15.
- Nakai S, Halliday AN and Rea DK (1993) Provenance of dust in the Pacific Ocean. *Earth and Planetary Science Letters* 119: 143–157.
- Nelson H and Creager JS (1977) Displacement of Yukon-derived sediment from Bering Sea to Chukchi Sea during Holocene time. *Geology* 5: 141–146.
- Nelson RE, Carter LD and Robinson SW (1988) Anomalous radiocarbon ages from a Holocene detrital organic lens in Alaska and their implications for radiocarbon dating and paleoenvironmental reconstructions in the Arctic. *Quaternary Research* 29: 66–71.
- Nurnberg D, Levitan MA, Pavlidis JA et al. (1995) Distribution of clay minerals in surface sediments from the eastern Barents and south-western Kara seas. *Geologische Rundschau* 84: 665–682.
- Nwaodua EC, Ortiz JD and Griffith EM (2014) Diffuse spectral reflectance of surficial sediments indicates sedimentary environments on the shelves of the Bering Sea and western Arctic. *Marine Geology* 355: 218–233.
- Ortiz JD, Nof D, Polyak L et al. (2012) The late Quaternary flow through the Bering Strait has been forced by the Southern Ocean winds. *Journal of Physical Oceanography* 42: 2014–2029.
- Ortiz JD, Polyak L, Grebmeier JM et al. (2009) Provenance of Holocene sediment on the Chukchi–Alaskan margin based on combined diffuse spectral reflectance and quantitative X-ray diffraction analysis. *Global and Planetary Change* 68: 73–84.
- Pin C and Santos Zalduegui JF (1997) Sequential separation of light-rare-earth elements, thorium and uranium by miniaturization extraction chromatography: Application to isotopic analyses of silicate rocks. *Analytica Chimica Acta* 339: 79–89.
- Polyak L, Darby DA, Bischof JF et al. (2007) Stratigraphic constraints on late Pleistocene glacial erosion and deglaciation of the Chukchi margin, Arctic Ocean. *Quaternary Research* 67: 234–245.



- Roach AT, Aagaard K, Pease CH et al. (1995) Direct measurements of transport and water properties through Bering Strait. *Journal of Geophysical Research* 100: 18443–18457.
- Sancetta CL, Hausser L, Labeyrie L et al. (1985) Wisconsin–Holocene paleoenvironment of the Bering Sea: Evidence from diatoms, pollen, oxygen isotopes and clay mineralogy. *Marine Geology* 62: 55–68.
- Stein R, Dittmers K, Fahl K et al. (2004) Arctic (paleo) river discharge and environmental change: Evidence from the Holocene Kara Sea sedimentary record. *Quaternary Science Reviews* 23: 1485–1511.
- Stigebrandt A (1987) The North Pacific: A global-scale estuary. *Journal of Physical Oceanography* 14: 464–470.
- Stokke PR and Carson B (1973) Variation in clay mineral X-ray diffraction results with the quantity of sample mounted. *Journal of Sedimentary Petrology* 43: 957–964.
- Stuiver M, Reimer PJ and Reimer RW (2017) CALIB 7.1 Available at: <http://calib.org>.
- Viscosi-Shirley C, Mammone K, Piasias N et al. (2003) Clay mineralogy and multi-element chemistry of surface sediments on the Siberian–Arctic shelf: Implications for sediment provenance and grain size sorting. *Continental Shelf Research* 23: 1175–1200.
- Wahsner M, Muller C, Stein R et al. (1999) Clay-mineral distributions in surface sediments from the Central Arctic Ocean and the Eurasian continental margin as indicator for source areas and transport pathways: A synthesis. *Boreas* 28: 215–233.
- Winter BL, Johnson CM and Clark DL (1997) Strontium, neodymium, and lead isotope variations of authigenic and silicate sediment components from the Late Cenozoic Arctic Ocean: implications for sediment provenance and the source of trace metals in seawater. *Geochimica et Cosmochimica Acta* 61: 4181–4200.
- Woodgate RA and Aagaard K (2005) Revising the Bering Strait freshwater flux into the Arctic Ocean. *Geophysical Research Letters* 32: L02602.
- Woodgate RA, Aagaard K and Weingartner TJ (2005) Monthly temperature, salinity, and transport variability of the Bering Strait through flow. *Geophysical Research Letters* 32: L04601.
- Yurco LN, Ortiz JD, Polyak L et al. (2010) Clay mineral cycles identified by diffuse spectral reflectance in Quaternary sediments from the Northwind Ridge: Implications for glacial–interglacial sedimentation patterns in the Arctic Ocean. *Polar Research* 29: 176–197.